Transfer characteristics of the hair cell's afferent synapse

Erica C. Keen and A. J. Hudspeth*

Howard Hughes Medical Institute and Laboratory of Sensory Neuroscience, The Rockefeller University, 1230 York Avenue, New York, NY 10021-6399

Contributed by A. J. Hudspeth, February 14, 2006

The sense of hearing depends on fast, finely graded neurotransmission at the ribbon synapses connecting hair cells to afferent nerve fibers. The processing that occurs at this first chemical synapse in the auditory pathway determines the quality and extent of the information conveyed to the central nervous system. Knowledge of the synapse's input–output function is therefore essential for understanding how auditory stimuli are encoded. To investigate the transfer function at the hair cell's synapse, we developed a preparation of the bullfrog's amphibian papilla. In the portion of this receptor organ representing stimuli of 400–800 Hz, each afferent nerve fiber forms several synaptic terminals onto one to three hair cells. By performing simultaneous voltage-clamp recordings from presynaptic hair cells and postsynaptic afferent fibers, we established that the rate of evoked vesicle release, as determined from the average postsynaptic current, depends linearly on the amplitude of the presynaptic Ca^{2+} current. This result implies that, for receptor potentials in the physiological range, the hair cell's synapse transmits information with high fidelity.

auditory system | exocytosis | glutamate | ribbon synapse | synaptic vesicle

The remarkable acuity and temporal precision of the auditory system are contingent on exocytosis at the hair cell's ribbon synapses, whose transfer characteristics are largely determined by the dependence of vesicle fusion on Ca^{2+} influx through voltage-gated channels. The relation of presynaptic voltage and Ca^{2+} influx to transmitter release at ribbon synapses is of particular interest in light of several unusual features of the hair cell's synaptic signaling. Afferent synapses encode inputs with graded membrane potentials (reviewed in ref. 1), transmit information with microsecond temporal fidelity (2), demonstrate multivesicular release (3–5), sustain high rates of exocytosis for prolonged periods (6–8), and display frequency tuning (9). Transmitter release is triggered by an atypical class of voltage-gated Ca^{2+} channels [noninactivating, L-type channels with α_{1D} principal subunits (10)] clustered at the presynaptic active zones (11–14). Finally, synaptotagmins I and II, the putative Ca^{2+} sensors for vesicle fusion in the brain, have not yet been detected at hair-cell synapses (15); instead, an alternative Ca^{2+} sensor, such as otoferlin (16), may effect exocytosis at these sites.

The operation of the hair cell's synapse has been investigated only indirectly by recording signals independently from either its presynaptic or postsynaptic element. Presynaptic measurements of membrane capacitance, an index of synaptic vesicle fusion, have provided information about the relation between presynaptic Ca^{2+} signals and vesicle release. Flash photolysis of caged Ca^{2+} indicates that the rate of exocytosis displays a fifth-order dependence on the cytoplasmic Ca^{2+} concentration (17), whereas hair-cell depolarization elicits vesicle release that is directly proportional to the presynaptic Ca^{2+} current (18, 19). Independent manipulation of either the number or the single-channel current of activated Ca^{2+} channels suggests that very few channels regulate the release of each synaptic vesicle (20). Exocytosis thus appears to be influenced by the Ca^{2+} concentration in the immediate vicinity of open channels rather than by the spatially averaged concentration originating from a cluster of channels. On the postsynaptic side, recordings of spontaneous excitatory postsynaptic currents (EPSCs) from the afferent nerve terminals of immature mammals have revealed a broad amplitude distribution suggestive of highly synchronized multivesicular release (3). Recordings of sound-evoked excitatory postsynaptic potentials and action potentials have elucidated other properties of information transfer across the synapse, including adaptation (21, 22) and frequency selectivity manifested by the sharp tuning curves and ready phase-locking of afferent fibers to low-amplitude stimuli (23).

Although these experiments have provided insight into the operation of the hair cell's synapse, it has not been possible to investigate directly the transfer characteristics of this synapse through simultaneous recordings from its pre- and postsynaptic elements. Such recordings offer the advantages of high temporal resolution, control over the presynaptic cell's voltage and intracellular milieu, and detection of only physiologically relevant vesicle release to the exclusion of that from outlying vesicles. We introduce here a preparation that permits such paired recordings, and we present data on the input–output function at the hair cell's afferent synapse.

Results

Experimental Preparation. We investigated the synaptic interaction between hair cells and afferent nerve fibers in the bullfrog's amphibian papilla. As the principal auditory receptor organ of anurans, the amphibian papilla detects airborne vibrations in the frequency range of 100–1,250 Hz. By controlled splitting of the sensory epithelium down its long axis, we exposed the unmyelinated afferent terminals innervating hair cells in the papilla's medial and caudal regions (Fig. 1*A*). Fracture ordinarily occurred along a row of hair cells lying near the midpoint of the organ's mediolateral axis. The frequency selectivity of both hair cells and afferent fibers defines a tonotopic gradient along the amphibian papilla (24–27). On the basis of this frequency map, the exposed cells would be expected to display characteristic frequencies of 400–800 Hz.

We used morphological techniques to characterize the innervation pattern in the region of interest. We immunolabeled hair cells with an antiserum directed against parvalbumin 3, an abundant cytoplasmic Ca^{2+} buffer, and afferent fibers with 3A10 monoclonal antibodies directed against neurofilament-associated proteins. The afferent terminals were typically 1–3 μm in diameter immediately postsynaptic to a hair cell and branched to contact one to three hair cells (Fig. 1*B*). Labeling of fibers and hair cells in the split epithelium confirmed that some of these synaptic contacts are preserved in the preparation used for electrical recording (Fig. 1*C*). To examine the trajectories of

Conflict of interest statement: No conflicts declared.

Freely available online through the PNAS open access option.

Abbreviations: AMPA, α-amino-3-hydroxy-5-methyl-4-isoxazolepropionic acid; EPSC, excitatory postsynaptic current.

*To whom correspondence should be addressed at: The Rockefeller University, Box 314, 1230 York Avenue, New York, NY 10021-6399. E-mail: hudspaj@rockefeller.edu.

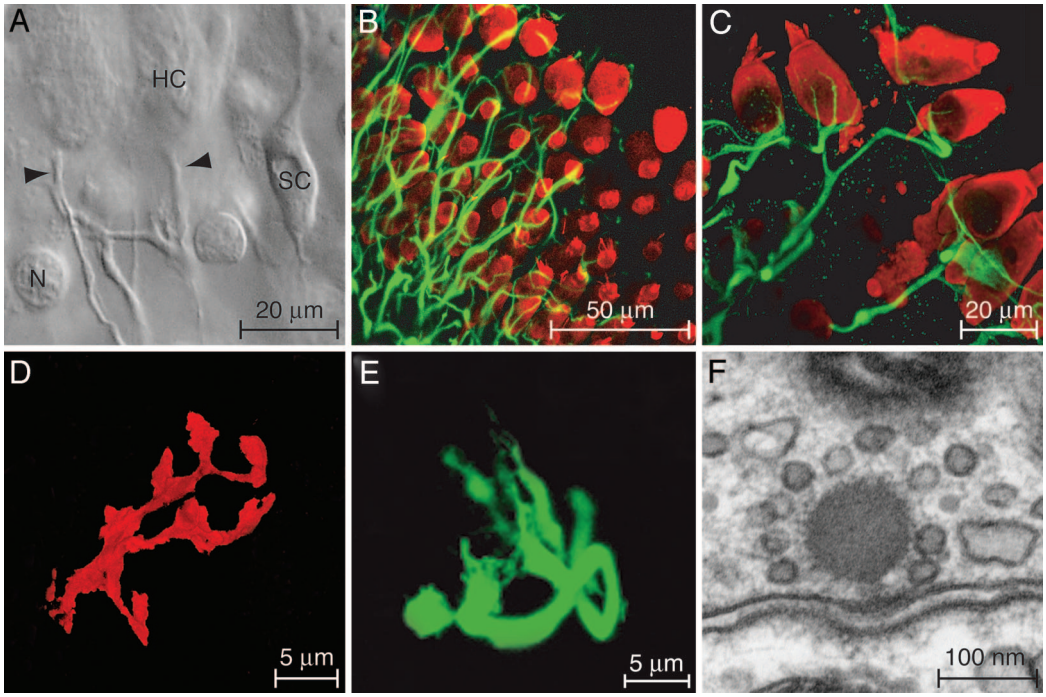

Fig. 1. *In vitro* preparation of the amphibian papilla. (*A*) A differential-interference-contrast micrograph depicts a portion of the split sensory epithelium in which the unmyelinated eighth-nerve fibers contact the basolateral surfaces of two hair cells (HC). Arrowheads, nerve terminals; SC, supporting cell; N, nucleus of dead supporting cell. (*B*) A stack of confocal images of the intact epithelium depicts hair cells immunolabeled for parvalbumin 3 (red) and afferent nerve terminals labeled for neurofilament-associated proteins (green). (*C*) A higher-magnification view of a split preparation shows the fine branches of afferent terminals juxtaposed to the basolateral surfaces of hair cells. (*D*) The terminal branches of a fiber labeled with a fluorescent lipophilic tracer surround a single hair cell. (*E*) An afferent terminal is labeled with a fluorescent tracer after whole-cell recording. (*F*) As visualized by transmission electron microscopy, an afferent synapse from the amphibian papilla displays prominent pre- and postsynaptic densities and an osmiophilic presynaptic dense body, or synaptic ribbon, to which a halo of synaptic vesicles is tethered.

individual afferent fibers, we labeled fibers terminating in the mid- to high-frequency portion of the sensory epithelium by diffusion of 1,1′-dioctadecyl-3,3,3′,3′-tetramethylindocarbocyanine perchlorate [diIC_{18}(3)] along the nerve bundle. In agreement with prior studies (24, 26), this approach demonstrated that each fiber in the region of interest branches only sparsely. In contradistinction to the one-to-one synaptic connectivity observed in the mammalian auditory periphery (28), however, each fiber terminates in multiple branches on a given hair cell (Fig. 1*D*). To examine the synaptic contacts more closely, we included in the recording pipettes a fluorophore that permitted cytoplasmic labeling of single afferent fibers. Confocal imaging confirmed that our electrical recordings originated from a fiber postsynaptic to a single hair cell and revealed the synaptic contacts terminating on that hair cell (Fig. 1*E*).

To investigate the fine structure of presynaptic active zones in the hair cells of interest, we performed electron microscopy on the mid- to high-frequency region of the amphibian papilla. In accordance with the general pattern of ribbon-type synapses in hair cells, including those in the papilla's rostral and caudal regions (29), each active zone displayed well defined presynaptic and postsynaptic densities and was marked by a prominent, ≈150-nm-diameter presynaptic dense body enveloped by synaptic vesicles (Fig. 1*F*).

Properties of EPSCs. Voltage-clamp recordings were obtained from afferent fibers near their terminations on the basolateral surfaces of hair cells in the mid- to high-frequency region of the amphibian papilla. Establishment of the whole-cell recording configuration was evident from the appearance of spontaneous EPSCs, which occurred at rates of 5–130 s^{-1} in control perilymph (Fig. 2*A*). The waveforms of these EPSCs were predominantly monophasic; however, a fraction of EPSCs, ≈5% in most recordings, displayed complex rise or decay waveforms (Fig. 2*B*). These multiphasic EPSCs were typically larger in amplitude than monophasic EPSCs. Spontaneous EPSCs recorded from an individual fiber showed a wide distribution of amplitudes, which varied over an order of magnitude (Fig. 2*C*). Although the smallest rise and decay times were observed for the smallest events, these kinetic parameters were not appreciably greater for larger events, suggesting that the release of multiple vesicles was highly synchronized (Fig. 2*D*). In a typical fiber recording, the mean 10–90% rise time for 700 spontaneous EPSCs smaller than 75 pA was 0.23 ± 0.09 ms, whereas the value for 363 events larger than 100 pA was 0.22 ± 0.10 ms. The mean decay time constant for the small EPSCs was 0.40 ± 0.08 ms and that for large EPSCs was 0.41 ± 0.06 ms. Although these recordings were postsynaptic to a single hair cell, they may have included EPSCs originating from several presynaptic active zones innervated by a branched afferent terminal. We therefore cannot determine in the current experimental configuration whether the multivesicular events represent release from a single presynaptic active zone.

Dependence of EPSCs on Glutamate Receptors. The small rise times and exponential decays of EPSCs accorded with the expected kinetics of currents mediated by glutamate receptors of the α-amino-3-hydroxy-5-methyl-4-isoxazolepropionic acid (AMPA) type in the auditory system (ref. 3 and reviewed in ref. 30). The rise and decay times of monophasic EPSCs were variable in individual fibers (Fig. 3*A*). For 3,944 EPSCs in three fibers held at −70 mV, the mean 10–90% rise time was 0.37 ± 0.28 ms, and the mean decay time constant was 0.59 ± 0.19 ms.

To investigate the voltage sensitivity of the postsynaptic responses, we recorded spontaneous EPSCs while a fiber was

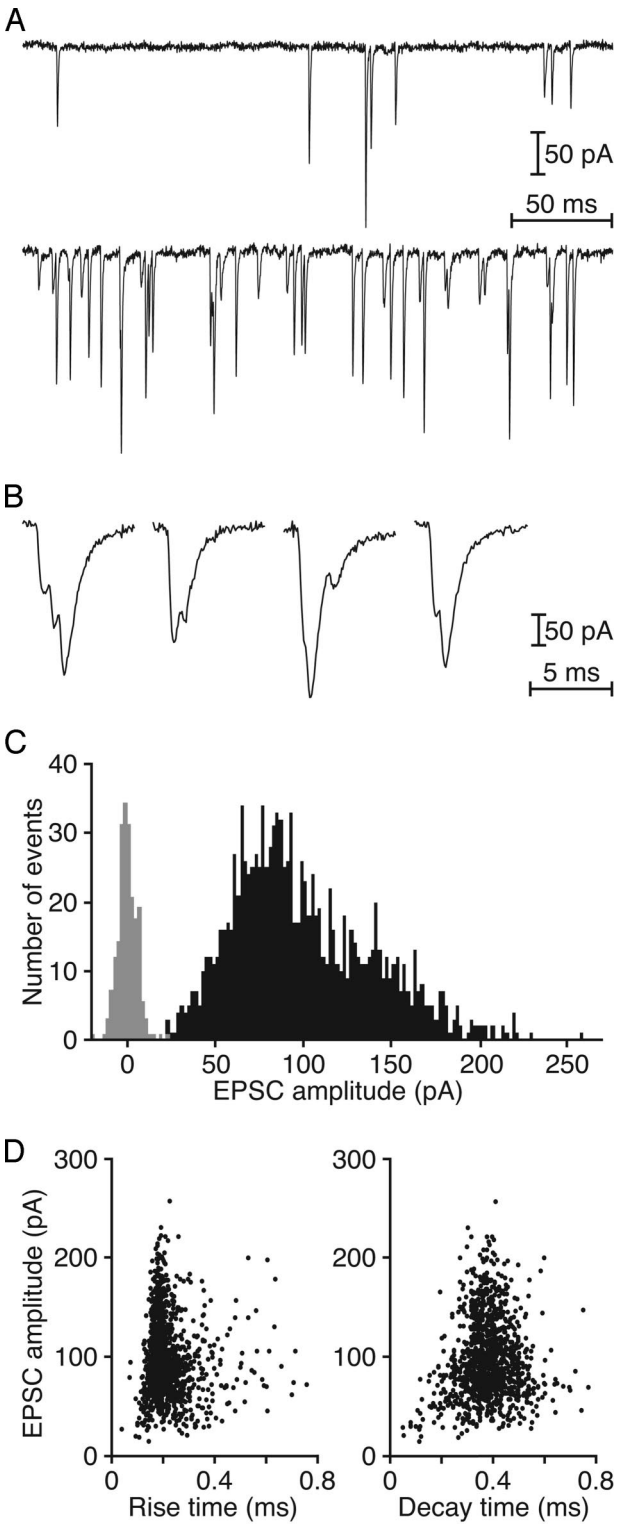

Fig. 2. Spontaneous EPSCs in afferent fibers. (*A*) The spontaneous EPSCs recorded from two terminals vary in amplitude and timing but display predominantly monophasic waveforms. (*B*) A subset of EPSCs display complex waveforms suggestive of multivesicular release slightly dispersed in time. (*C*) The amplitude distribution of spontaneous EPSCs (black) recorded in a particular afferent fiber extends over more than one order of magnitude. Analysis of these 1,216 events showed a mean amplitude of 100 ± 39 pA and an occurrence rate of 24 s^{-1}. The scaled distribution of noise amplitudes is shown in gray. (*D*) The 10–90% rise times (*Left*) and time constants of decay (*Right*) for EPSCs from the same fiber display tight distributions, suggesting that multiple release events are highly synchronized.

maintained at holding potentials from −100 mV to +50 mV. The kinetics and amplitudes of spontaneous EPSCs were voltage-dependent; the responses slowed at more positive potentials and reversed sign near 0 mV (Fig. 3*B*). Cyclothiazide, an agent that reduces the desensitization of AMPA receptors, doubled the decay time constant of EPSCs (Fig. 3*C*). Application of 6-cyano-7-nitroquinoxaline-2,3-dione (CNQX), an antagonist of AMPA and kainate receptors, completely and reversibly blocked EPSCs (Fig. 3*D*). These results indicate that EPSCs at the amphibian papilla's afferent synapse are mediated by AMPA receptors.

Dependence of EPSCs on Ca^{2+} Influx Through L-Type Channels. When added to the external solution, nifedipine, a specific antagonist of L-type voltage-gated Ca^{2+} channels, reversibly abolished spontaneous EPSCs (Fig. 3*E*). The release of synaptic transmitter therefore depends on Ca^{2+} influx through L-type Ca^{2+} channels, which is consistent with recordings from primary auditory afferent neurons showing that both spontaneous and sound-evoked transmitter release are sensitive to dihydropyridines (14).

Paired Recordings. To determine directly the dependence of the postsynaptic response on the presynaptic membrane potential, and especially on the presynaptic Ca^{2+} current, we performed paired voltage-clamp recordings on hair cells and afferent fibers. A recording was first obtained from an afferent fiber near its termination on the basolateral surface of a hair cell. In a total of six instances, we were then able to make a simultaneous whole-cell recording from the innervated hair cell. In five of these cases, the afferent fiber contacted solely the voltage-clamped hair cell, as verified by fluorescent dye labeling of the fiber and by the near elimination of postsynaptic currents when the hair cell was hyperpolarized to −80 mV.

After the two simultaneous recordings had been established, we explored the relationship between presynaptic voltage and vesicle release by stepping the hair cell's membrane potential from a holding level of −80 mV to test values between −70 mV and +10 mV. Evoked EPSCs were observed during the presentation of depolarizing pulses and persisted for the duration of each stimulus (Fig. 4). The rate of release did not necessarily remain constant; EPSCs in some experiments displayed adaptive changes during large presynaptic depolarizations, and in others showed an increase in rate suggestive of a progressive accumulation of cytoplasmic Ca^{2+}. The evoked EPSCs of some cell pairs were superimposed, precluding comparative analysis of the amplitude distributions of spontaneous and evoked currents from such fibers. In two of the paired recordings, however, individual EPSCs were discernible during maximal presynaptic stimulation. The amplitudes of the largest evoked EPSCs under these circumstances did not exceed those of the largest spontaneous EPSCs (data not shown).

We were also able to investigate the relationship between presynaptic Ca^{2+} influx and vesicle release by using the voltage-step protocol. Depolarizing voltage pulses activated an inward current in the hair cell and evoked EPSCs in the afferent fiber (Fig. 5*A*). The presynaptic inward current revealed with a Cs^{+}-based internal solution was noninactivating and nifedipine-sensitive, which, together with its voltage–current relation, signified Ca^{2+} influx through L-type Ca^{2+} channels (data not shown).

As a measure of the postsynaptic response, we integrated the evoked EPSC and divided the result by the duration of the depolarizing stimulus. This average postsynaptic current was presumably proportional to the number of glutamate receptors that bound the released transmitter, and in turn to the number of synaptic vesicles that liberated their contents. The postsynaptic current depended on the hair cell's membrane potential and mirrored the steep voltage dependence of the presynaptic

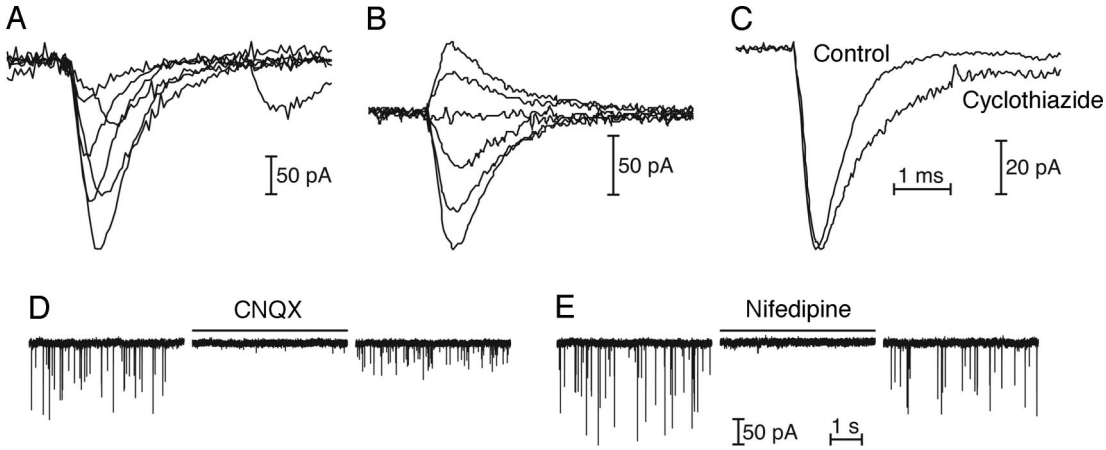

Fig. 3. Spontaneous EPSCs mediated by AMPA receptors. (*A*) Superimposed records from one fiber reveal the rapid onset and slower, exponential decay of monophasic EPSCs, as well as the variation in rise time. (*B*) As the postsynaptic membrane potential was varied, averaged EPSCs reversed sign near 0 mV and slowed at more positive potentials. From top to bottom, the holding potentials were +50 mV, +30 mV, 0 mV, −20 mV, −70 mV, and −100 mV. (*C*) Addition of 100 μM cyclothiazide halved the average decay rate of spontaneous EPSCs, increasing the time constant from 0.65 ± 0.13 ms (n = 91) to 1.25 ± 0.27 ms (n = 38). (*D*) An antagonist of AMPA and kainate receptors, 6-cyano-7-nitroquinoxaline-2,3-dione (CNQX), reversibly blocked EPSCs at a concentration of 10 μM. (*E*) Nifedipine, a specific antagonist of L-type Ca^{2+} channels, reversibly blocked EPSCs at a concentration of 50 μM.

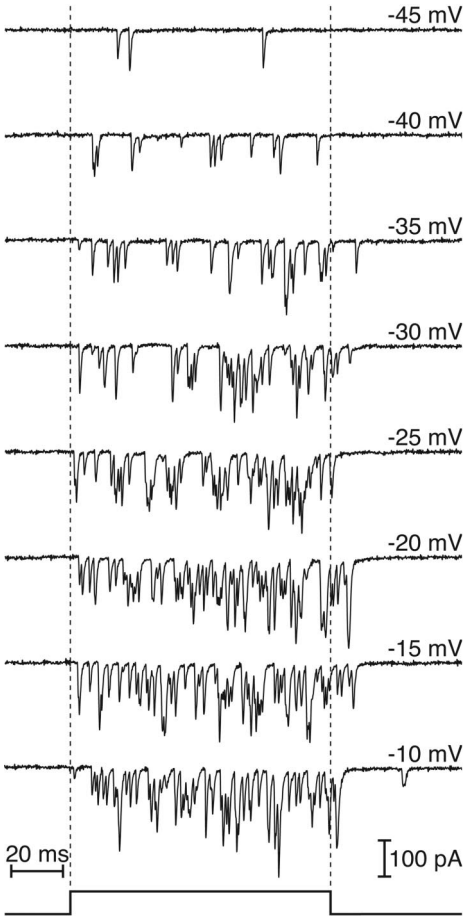

Fig. 4. Relationship between presynaptic voltage and evoked EPSCs. In a simultaneous voltage-clamp experiment, the hair cell was confronted with a series of 100-ms depolarizations whose timing is displayed at the bottom of the figure. For depolarizations that evoked near-maximal Ca^{2+} currents, the latency between stimulus onset and the first response decreased, and evoked EPSCs persisted after the termination of the pulse.

Ca^{2+} current (Fig. 5*B*). The Ca^{2+} current activated near −55 mV and was maximal at −20 mV; similarly, the postsynaptic current displayed an activation threshold between −55 mV and −50 mV and peaked at −20 mV to −10 mV.

At the presynaptic active zones of hair cells, the local Ca^{2+} concentration is expected to be directly proportional to the Ca^{2+} current (31). To determine the dependence of synaptic release on Ca^{2+}, we therefore plotted the average amplitude of the postsynaptic current against the presynaptic Ca^{2+} current at each test potential. Both signals displayed considerable variation between cell pairs, perhaps as a consequence of the heterogeneous electrical properties of amphibian papilla hair cells (27) and differences in the number of postsynaptic AMPA receptors. Nevertheless, the data from five sets of recordings were well approximated by linear fits over a range of presynaptic potentials that corresponds to physiological stimulation (Fig. 5*C*). In some instances, the average postsynaptic current saturated as the presynaptic Ca^{2+} current increased still further.

Discussion

Paired Recordings at Hair-Cell Afferent Synapses. Investigation of the input–output function at ribbon synapses in the auditory system is critical for understanding the mechanisms by which the electrical responses of hair cells are translated into a neural spike code. The split sensory epithelium of the bullfrog's amphibian papilla permits the study of synaptic signaling across this first synapse in the auditory pathway. The preparation preserves functional synapses in the epithelium yet exposes postsynaptic terminals for electrophysiological analysis. By using this preparation, it is possible to study not only spontaneous vesicle release from hair cells but also the transfer characteristics of the synapse with paired whole-cell recordings. Because this experimental preparation originates from an adult animal, its properties presumably reflect mature synaptic transmission. That no enzyme is used during the dissection or recording procedures further ensures the normal operation of the synapse.

Properties of EPSCs. The spontaneous EPSCs that we observed in afferent fibers of the amphibian papilla are consistent with anatomical observations of membrane recycling at unstimulated active zones and with physiological observations of spontaneous firing in eighth-nerve fibers (32, 33). The waveforms and phar-

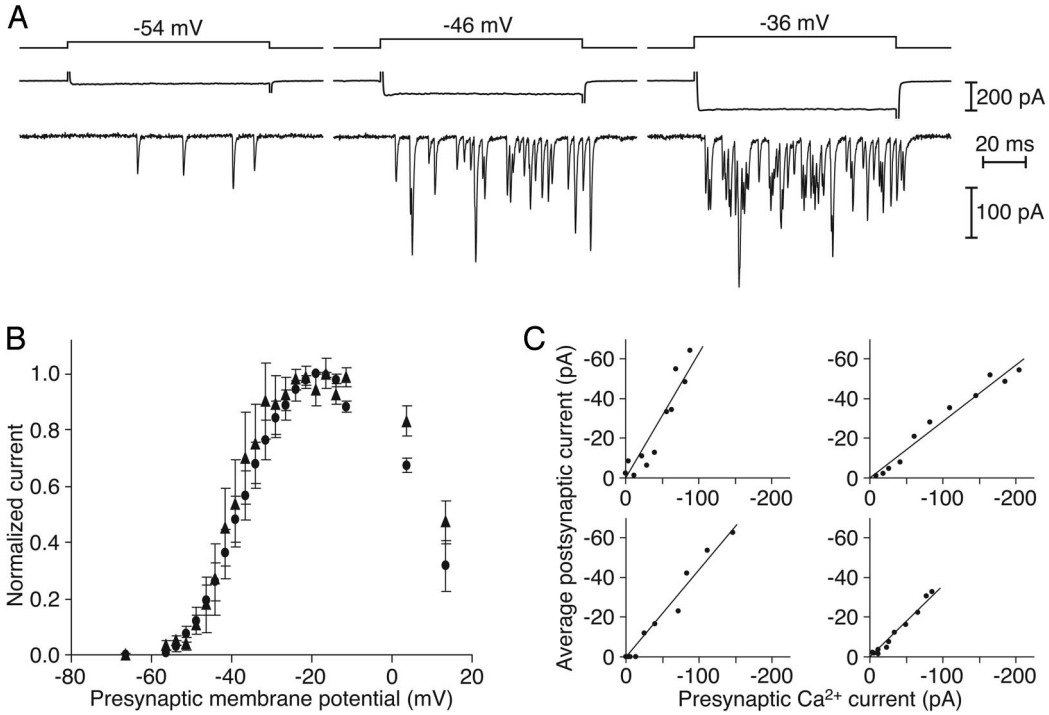

Fig. 5. Voltage and Ca^{2+} sensitivity of transmitter release. (*A*) Recordings during a simultaneous voltage-clamp experiment depict presynaptic Ca^{2+} currents (middle traces) and EPSCs (bottom traces) evoked by 100-ms hair-cell depolarizations (top traces). (*B*) Both the presynaptic Ca^{2+} current (circles) and the postsynaptic current (triangles) display a sigmoidal dependence on the test potential. Data are presented as normalized means ± standard errors of the means for four experiments. (*C*) In each of four paired recordings, the dependence of the postsynaptic current on the presynaptic Ca^{2+} current is approximately linear over a physiologically relevant range of hair-cell membrane potentials, here −56 mV to −31 mV. Clockwise from the upper left, the linear regression coefficients (r^2) are 0.88, 0.97, 0.97, and 0.95.

macological sensitivities of these currents accord with evidence that synaptic transmission at mammalian auditory ribbon synapses is mediated by AMPA-type glutamate receptors with rapid kinetics (3). The broad amplitude distributions of EPSCs from individual fibers suggest that multiple vesicles are released, whether from single or from multiple active zones, with a high degree of temporal precision.

Input–Output Function at Hair-Cell Synapses. Despite nonlinear stimulus processing in both the presynaptic hair cell and the postsynaptic afferent fiber, the intervening synapse evidently operates in a linear regime under our experimental conditions. Such a relationship has also been observed for the ribbon synapses of rod photoreceptors, at which the linearity between presynaptic Ca^{2+} signals and vesicle fusion facilitates the encoding of small changes in illumination (34). In several auditory receptor organs, presynaptic vesicle fusion has been shown to depend linearly on the presynaptic Ca^{2+} current (18, 19). The present demonstration that this linear relation extends across the synapse to the postsynaptic current implies that the postsynaptic receptors faithfully transmit the information conveyed by hair-cell exocytosis.

In most instances, the postsynaptic response vanished at potentials more negative than −55 mV despite the persistence of a small Ca^{2+} current (Fig. 5*C*). This result is consistent with evidence that exocytosis displays a higher-order Ca^{2+} dependence at the threshold of synaptic responsiveness (17). Near the normal resting potential of −55 mV to −50 mV for hair cells of the amphibian papilla (35, 36), however, the linear relation was obtained consistently. In many receptor organs, including the amphibian papilla (27, 36), the responsiveness of hair cells is accentuated by resonant electrical tuning mediated by colocalized Ca^{2+} channels and Ca^{2+}-activated K^+ channels. Analysis of the ionic currents underlying this process indicates that the presynaptic Ca^{2+} current closely follows the membrane potential (37). Linearity at the afferent synapse therefore ensures that responses sharpened by electrical resonance are faithfully propagated to the afferent nerve fiber. More generally, we propose that the direct proportionality of vesicle release, and also the postsynaptic current as observed in our experiments, to Ca^{2+} influx facilitates the encoding of auditory stimuli by allowing the synapse to be sensitive to low-amplitude stimuli, to possess a wide dynamic range for finely graded intensity discrimination, and to transfer complex waveforms with minimal distortion.

Materials and Methods

Experimental Preparation. Amphibian papillae were dissected from adult bullfrogs (*Rana catesbeiana*) that had been sedated by cold, doubly pithed, and decapitated. Papillae were maintained in oxygenated artificial perilymph containing 120 mM NaCl, 2 mM KCl, 1–2 mM $CaCl_2$, 3 mM D-glucose, 1 mM creatine, 1 mM sodium pyruvate, and 5 mM Hepes at pH 7.25 (230 mosmol·kg^{-1}). Amiloride (100 μM) was included during the dissection to block mechanoelectrical transduction channels and thereby lessen Ca^{2+}-mediated excitotoxicity.

After the sensory epithelium had been exposed by cutting and folding back the papilla's cartilaginous roof, the overlying tectorial membrane was removed with fine forceps. The papilla was positioned on a 125-μm-diameter tungsten wire such that its tonotopic axis paralleled the wire. When the preparation was stretched against the wire by securing it at four locations, the opposing forces applied to the cartilaginous roof and to the tissue beneath the main nerve bundle exerted stress on the sensory epithelium. The resulting strain usually split the epithelium along its tonotopic axis, exposing afferent fibers at their terminations on hair cells.

Electrophysiology. Hair cells and afferent fibers were visualized by differential-interference-contrast video microscopy with a ×63 water-immersion objective lens, ×5 optical magnification, and ×2 digital magnification. Whole-cell, voltage-clamp recordings were performed with two Axopatch 200A amplifiers (Axon Instruments, Union City, CA). Stimuli were presented and data acquired with programs written in LABVIEW (National Instruments, Austin, TX). Currents were low-pass filtered at 8 kHz and sampled at 50-μs intervals. During afferent fiber recordings, 1 μM tetrodotoxin was included in the perilymph to block voltage-gated Na^+ channels.

Recordings were obtained at room temperature with borosilicate glass pipettes pulled to resistances of 2–4 MΩ for hair-cell recordings and 8–10 MΩ for afferent fiber recordings. The internal solution for both recordings contained 110 mM CsCl, 0.5 mM $MgCl_2$, 2 mM EGTA, 5 mM Na_2ATP, and 10 mM Hepes at pH 7.3 (230 mosmol·kg^{-1}). A Cs^+-based internal solution was used to permit measurement of the presynaptic Ca^{2+} current, block some nonlinear K^+ conductances, and increase the postsynaptic input resistance. We chose not to introduce further blocking agents that might interfere with vesicle release; therefore, the presynaptic Ca^{2+} current was sometimes contaminated by the presence of residual, outward K^+ currents. Because these K^+ currents activated slowly, however, the initial peak inward current accurately reflected the magnitude of the Ca^{2+} current and was used for analysis. To assess the configuration of terminals from which we had recorded by confocal microscopy (LSM-510; Zeiss), we included the fluorophore Alexa 488 hydrazide at 50 μM in the postsynaptic internal solution.

Afferent terminals were held at a potential of −70 mV during postsynaptic recordings. For paired recordings, hair cells were maintained at −80 mV between stimulus presentations. Holding potentials were corrected post hoc for a 4-mV junction potential but not for the voltage drop across the uncompensated series resistance. Because the Ca^{2+} current in hair cells never exceeded 300 pA, this voltage error was at most 2 mV. The input resistances of afferent terminals measured 250–500 MΩ; the fibers' input capacitances were 1–4 pF. When measured in current-clamp mode, the resting potentials of afferent fibers were stable at −75 mV to −55 mV for up to 45 min of recording.

Data Analysis. The total charge transfer associated with each evoked postsynaptic current was calculated by integrating the change in the postsynaptic current during the presentation of a 100-ms test potential. The average postsynaptic current was defined as the total charge transfer divided by the duration of the stimulus. Data analysis was performed with MINIANALYSIS (SYNAPTOSOFT; Jaejin Software, Leonia, NJ), EXCEL (Microsoft), and MATHEMATICA (Wolfram Research, Champaign, IL). Unless otherwise noted, statistical results are reported as means ± standard deviations.

We thank Mr. B. Fabella for computer programming and Mr. A. Hinterwirth for the construction of apparatus. Dr. H. von Gersdorff, Dr. W. M. Roberts, and the members of our research group provided valuable comments on the manuscript. This work was supported by National Institutes of Health Grants DC00241 and GM07739. A.J.H. is an investigator of the Howard Hughes Medical Institute.

1. Prescott, E. D. & Zenisek, D. (2005) *Curr. Opin. Neurobiol.* **15,** 431–436.
2. Sullivan, W. E. & Konishi, M. (1984) *J. Neurosci.* **4,** 1787–1799.
3. Glowatzki, E. & Fuchs, P. A. (2002) *Nat. Neurosci.* **5,** 147–154.
4. Edmonds, B. W., Gregory, F. D. & Schweizer, F. E. (2004) *J. Physiol. (London)* **560,** 439–550.
5. Singer, J. H., Lassova, L., Vardi, N. & Diamond, J. S. (2004) *Nat. Neurosci.* **7,** 826–833.
6. Moser, T. & Beutner, D. (2000) *Proc. Natl. Acad. Sci. USA* **97,** 883–888.
7. Eisen, M. D., Spassova, M. & Parsons, T. D. (2004) *J. Neurophysiol.* **91,** 2422–2428.
8. Griesinger, C. B., Richards, C. D. & Ashmore, J. F. (2005) *Nature* **435,** 212–215.
9. Rutherford, M. A. & Roberts, W. M. (2006) *Proc. Natl. Acad. Sci. USA* **103,** 2898–2903.
10. Kollmar, R., Montgomery, L. G., Fak, J., Henry, L. J. & Hudspeth, A. J. (1997) *Proc. Natl. Acad. Sci. USA* **94,** 14883–14888.
11. Roberts, W. M., Jacobs, R. A. & Hudspeth, A. J. (1990) *J. Neurosci.* **10,** 3664–3684.
12. Issa, N. P. & Hudspeth, A. J. (1994) *Proc. Natl. Acad. Sci. USA* **91,** 7578–7582.
13. Platzer, J., Engel, J., Schrott-Fischer, A., Stephan, K., Bova, S., Chen, H., Zheng, H. & Streissnig, J. (2000) *Cell* **102,** 89–97.
14. Robertson, D. & Paki, B. (2002) *J. Neurophysiol.* **87,** 2734–2740.
15. Safieddine, S. & Wenthold, R. J. (1999) *Eur. J. Neurosci.* **11,** 803–812.
16. Mirghomizadeh, F., Pfister, M., Apayden, F., Petit, C., Kupka, S., Pusch, C. M., Zenner, H.-P. & Blin, N. (2002) *Neurobiol. Dis.* **10,** 157–164.
17. Beutner, D., Voets, T., Neher, E. & Moser, T. (2001) *Neuron* **29,** 681–690.
18. Johnson, S. L., Marcotti, W. & Kros, C. J. (2005) *J. Physiol. (London)* **563,** 177–191.
19. Schnee, M. E., Lawton, D. M., Furness, D. N., Benke, T. A. & Ricci, A. J. (2005) *Neuron* **47,** 243–254.
20. Brandt, A., Khimich, D. & Moser, T. (2005) *J. Neurosci.* **25,** 11577–11585.
21. Furukawa, T., Hayashida, Y. & Matsuura, S. (1978) *J. Physiol. (London)* **276,** 211–226.
22. Furukawa, T., Kuno, M. & Matsuura, S. (1982) *J. Physiol. (London)* **322,** 181–195.
23. Köppl, C. (1997) *J. Neurosci.* **17,** 3312–3321.
24. Lewis, E. R., Leverenz, E. L. & Koyama, H. (1982) *J. Comp. Physiol.* **145,** 437–445.
25. Yu, X., Lewis, E. R. & Feld, D. (1991) *J. Comp. Physiol. A* **169,** 241–248.
26. Simmons, D. D., Bertolotto, C. & Narins, P. M. (1992) *J. Comp. Neurol.* **322,** 191–200.
27. Smotherman, M. S. & Narins, P. M. (1999) *J. Neurosci.* **19,** 5275–5292.
28. Liberman, M. C. (1980) *Hear. Res.* **3,** 45–63.
29. Simmons, D. D., Bertolotto, C. & Leong, M. (1995) *Aud. Neurosci.* **1,** 183–193.
30. Trussell, L. O. (1999) *Annu. Rev. Physiol.* **61,** 477–496.
31. Roberts, W. M. (1994) *J. Neurosci.* **14,** 3246–3262.
32. Lenzi, D., Runyeon, J. W., Crum, J., Ellisman, M. H. & Roberts, W. M. (1999) *J. Neurosci.* **19,** 119–132.
33. Sewell, W. F. (1984) *J. Physiol. (London)* **347,** 685–696.
34. Thoreson, W. B., Rabl, K., Townes-Anderson, E. & Heidelberger, R. (2004) *Neuron* **42,** 595–605.
35. Pitchford, S. & Ashmore, J. F. (1987) *Hear. Res.* **27,** 75–83.
36. Ospeck, M., Eguíluz, V. M. & Magnasco, M. O. (2001) *Biophys. J.* **80,** 2597–2607.
37. Hudspeth, A. J. & Lewis, R. S. (1988) *J. Physiol. (London)* **400,** 275–297.